COMMUNICATION

The combined use of gold nanoparticles and infrared radiation enables cytosolic protein delivery

Josep Garcia,[a] J. Marcos Fernández-Pradas,[b,c] Anna Lladó,[a] Pere Serra,[b,c] Dobryna Zalvidea,[d] Marcelo J. Kogan,[e,f] Ernest Giralt,*[a,g] Macarena Sánchez-Navarro*[a]

[a] Dr. J. Garcia, Dr. A. Lladó, Dr. E.Giralt, Dr. M. Sánchez Navarro
Institute for Research in Biomedicine-Barcelona Institute of Science and Technology,
Baldiri Reixac 10, 08028 Barcelona, Spain.
E-mail: ernest.giralt@irbbarcelona.org; macarena.sanchez@irbbarcelona.org
[b] Dr. J. M. Fernández-Pradas, Dr. Pere Serra
Department of Applied Physics, University of Barcelona,
Martí i Franquès 1, 08028, Barcelona, Spain.
[c] Dr. J. M. Fernández-Pradas, Dr. Pere Serra
Institute of Nanoscience and Nanotechnology (IN2UB), University of Barcelona,
Av. Diagonal 645, 08028, Barcelona, Spain.
[d] Dr. D. Zalvidea
Institute for Bioengineering of Catalonia (IBEC), The Barcelona Institute of Technology (BIST),
Barcelona, Spain.
[e] Dr. M. J. Kogan
Departamento de Química Farmacológica y Toxicológica, Facultad de Ciencias Químicas y Farmacéuticas, Universidad de Chile,
Santiago, Chile.
[f] Dr. Dr. M. J. Kogan
Advanced Center for Chronic Diseases (ACCDiS),
Sergio Livingstone 1007, Independencia,
Santiago, Chile.
[g] Prof. E. Giralt
Department of Inorganic and Organic Chemistry, University of Barcelona,
Martí i Franquès 1-11, Barcelona 08028, Spain

Supporting information for this article is given via a link at the end of the document.

Abstract: Cytosolic protein delivery remains elusive. The inability of most proteins to cross the cellular membrane is a huge hurdle. Here we explore the unique photothermal properties of gold nanorods (AuNRs) to trigger cytosolic delivery of proteins. Both partners, protein and AuNRs, are modified with a protease-resistant cell-penetrating peptide with nuclear targeting properties to induce internalization. Once internalised, spatiotemporal control of protein release is achieved by near-infrared laser irradiation in the safe second biological window. Importantly, catalytic amounts of AuNRs are sufficient to trigger cytosolic protein delivery. To the best of our knowledge, this is the first time that AuNRs with their maximum of absorption in the second biological window are used to deliver proteins into the intracellular space. This strategy represents a powerful tool for the cytosolic delivery of virtually any class of protein.

Proteins and peptides hold great potential to interfere in biological processes, both extra and intracellularly, at low concentration and with great selectivity. Recent advances in protein production and a deeper understanding of cell biology have led to the development of protein tools with many applications in basic and applied research.[1] However, proteins are hampered by low stability and poor cell penetration. Numerous strategies are used to tackle these limitations. Stability issues are partially solved by chemical modifications such as PEGylation.[2] Conversely, the development of intracellular delivery strategies of functional biomolecules remains elusive.[3] Several approaches have been proposed such as electroporation,[4] protein engineering to increase pKa (supercharged proteins),[5] nanoparticle (NP) formulation[6] and the use of peptide-mediated delivery.[7] Cell-penetrating peptides (CPPs) emerged as a revolution in the field, but deeper analysis of the results revealed that most CPPs led to endosomal entrapment of the attached cargoes.[8–10] Various reagents, such as chloroquine, can be used to promote endo-lysosomal membrane disruption.[11] More recent approaches include the use of cyclic CPPs[12] or endosomolytic peptides,[13,14] which act either by escaping the endocytic route of entry or by destabilising the endosomal vesicles.[15] NPs, of diverse type, represent another platform to deliver proteins offering also a great platform to incorporate other molecules, such as targeting moieties or even additional drugs.[6] However, none of these approaches allows for the spatial and temporal control of the intracellular release of the compound of interest. Other strategies, such as the so-called photochemical internalization overcome this issue by using photosensitisers that would induce membrane disruption upon irradiation.[16] Conversely, their use is limited to the visible region of the spectra. [17] In this context, near infra-red (NIR)-activable materials have several advantages.[18] On the one hand, they allow for remote control with spatiotemporal precision.[19] On the other hand, they show low toxicity. In particular, plasmonic nanoparticles such as gold nanorods (AuNRs), nanoshells or nanocages, offer

great potential,[20] since irradiation at the surface plasmon resonance (SPR) frequency results in light-to-heat energy conversion that can lead to localised heating.[21] NIR irradiation is compatible with tissue in two regions, namely the first biological window, which ranges from 650 to 950 nm, and in the second biological window, which ranges from 1000 to 1300 nm. Importantly, gold nanostructures properties can be tuned to work at the second biological window, in which water absorption is minimal, thereby resulting in deeper tissue penetration with minimal collateral heating.[22] Of all gold nanostructures, AuNRs display the highest optical cross-section and the highest absorption efficiency, thus resulting in good photothermal properties when irradiated with low laser energy.[23]

These outstanding properties of AuNRs have been used to deliver biomacromolecules, specially siRNA, to the cytosol.[18,24,25] In most cases the NP acts as a carrier, requiring surface modification to attach the cargo either covalently or by electrostatic interactions, and light activation is used to trigger cell death. The combined use of photothermic therapy and gene silencing has proven to be more efficient than the use of the treatments separately. Ferreira *et. al*, took advantage of the ease of gold functionalization to attach two distinct proteins to the nanorod surface via DNA hybridization. Consecutive irradiation at controlled intensity resulted in sequential delivery of the active form of the proteins.[26]

Despite advances in the field, the use of the photothermal properties of gold nanomaterials to deliver proteins to the cytosol has been explored only in the first biological window.[18] In this work, we propose the use of AuNRs to trigger the endosomal escape of proteins. We hypothesise that modification of AuNRs and the protein of interest with the same CPP will induce the cell entry of both entities by the same mechanisms and that they will end up in the same intracellular compartment. Light activation of the AuNR results in controlled localised heating that can lead to endosomal disruption. In this case, the protein is released in the cytosolic space before undergoing proteolytic degradation. As proof-of-concept, we have modified both the protein and AuNR with an all-D CPP, r_8, to make them cell permeable.[27] Light activation results in endosomal disruption via photothermal effect with spatial and temporal control. Since r_8 has nuclear targeting properties, the modified protein was directed to the nucleus, especially to the nucleolus.[28] We believe that this is the first time that AuNRs with their longitudinal SPR (LSPR) band at the second biological window are used to promote cytosolic delivery of proteins.

Results and discussion

Our first aim was to synthesise AuNRs with their LSPR band in the second NIR window, to efficiently use radiation with deeper tissue penetration capability. To this end, a modified seeding growth method was used (Fig. S1).[29] AuNRs were obtained at high purity (>93%, compared to other side-products), displaying a LSPR maximum peak at 1001 nm and an aspect ratio of 5.6; comprising a length value of 50.7 ± 7.7 nm and width of 9.0 ± 0.7 nm, as measured by transmission electron microscopy (TEM) (Fig. 1 and S2).

Hexadecyltrimethylammonium bromide (CTAB) was used to favour the formation of rod shape NPs and to stabilise the colloidal solution.[30] However, it results in a high cytotoxicity.[31] PEGylation is a strategy widely used to stabilise AuNRs, preventing aggregation, reducing NP toxicity and increasing biocompatibility.[32]

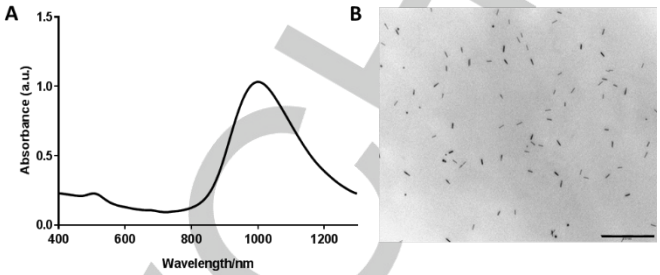

Fig. 1. Characterization of AuNRs: A) UV-Vis-IR Spectrum. LSPR band maximum at 1001 nm. B) Transmission electron micrograph. Scale bar 500 nm.

Therefore, CTAB was removed from the AuNR surface by means of the ligand-exchange method using a combination of two bifunctional PEGs, namely methoxy-PEG-thiol (mPEG, Mw: 5000 Da) and carboxy-PEG-thiol (cPEG, Mw: 5000 Da). The methoxy group confers stability to the rods and the carboxyl group allows the further incorporation of ligands.

To promote cell internalization via endocytosis, r_8, a widely used CPP, was selected to functionalise the exposed carboxyl groups displayed on the AuNR surface.[33] The non-natural amino acids of the sequence ensure peptide stability in front of serum proteases without compromising cell internalization properties. Polyarginines have been used to promote the uptake of drugs, polymeric NP and proteins, among others.[12,34,35], The mechanism of cell internalization used by these molecules depends on the length of the polyarginine chain and on the cargo attached, ranging from macropinocytosis to caveolin- or clathrin-mediated endocytosis[9,36] This family of CPPs has scarcely been used to promote AuNR translocation. Direct functionalization of AuNRs with CR_8 was used to promote apoptosis or necrosis of macrophages upon irradiation.[37] More recently, we reported that the modification of AuNR with R_7 or R_7CLPFFD improves the interaction of AuNRs with biological membranes (liposomes), as well as their internalization in mammalian cells, without affecting cell viability.[38]

In the present study, a fluorescently labelled version of r_8 was used (carboxyfluorescein, r_8-k(cF)) to confirm AuNRs internalization. The peptide was prepared using solid-phase peptide synthesis (Scheme S1, Fig. S3) and introduced into the AuNRs via an amide bond. The carboxyl groups displayed at the AuNR surface were first activated with *N*-(3-Dimethylaminopropyl)-N′-ethylcarbodiimide hydrochloride (EDC·HCl) and sulfo-*N*-Hydroxysuccinimide (s-NHS), followed by the addition of fluorescently labelled peptide r_8-k(cF). The excess of peptide and reagents was removed by centrifugation. The modified AuNRs (AuNR-PEG-r_8-k(cF)) were characterised by UV-VIS, Z-potential and amino acid analysis. The LSPR band of the modified systems showed a negligible shift, suggesting minor or no aggregation after modifications (Fig. S4). The Z-potentials of AuNR-PEG-r_8-k(cF) and AuNR-PEG-r_8-k were -9.06 ± 3.19 and -6.60 ± 1.57

mV, respectively, while unmodified AuNRs displayed a Z-potential of 21.0 ± 1.39 mV. This reduction in surface charge is consistent with substitution of the CTAB molecules from the AuNR surface. Finally, the number of peptides per AuNR, as determined by amino acid analysis, was 1038 ± 16 for r_8-k(cF) and 1077 ± 24 for r_8. This number is consistent considering the size of the AuNR.[39,40]

We next examined the heating capacity and photothermal stability of modified and unmodified AuNRs (Fig 2, S5). To this end, we have used a continuous wave (CW) NIR laser source.

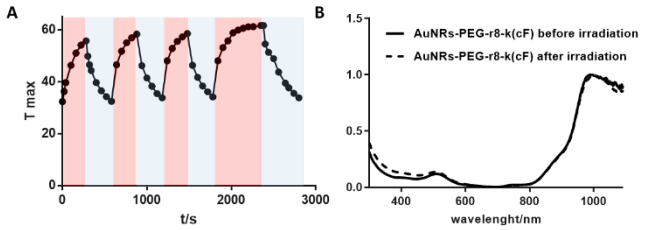

Fig. 2. A) Temperature increase of AuNR-PEG-r_8-k(cF) aqueous dispersion for four laser on/off cycles; B) Absorption spectra of AuNRs aqueous dispersion before and after the laser irradiation.

The temperature of the AuNR-PEG-r_8-k(cF) solution was monitored during laser irradiation (1064 nm, 4.5 W/cm^2) for 5 min, followed by 5 min of cooling (laser off). This cycle was repeated 3 times. As shown in Fig. 2A, the photothermal effect of AuNR-PEG-r_8-k(cF) was maintained during the cycles. Also, UV-VIS-NIR spectra recorded after irradiation revealed a minor shift in the case of unmodified AuNRs (Fig. S5B) and no shift in the case of the modified ones, which is explained by the stabilizing effect of PEG modification (Fig 2B). The conservation of the UV-VIS-NIR spectra of this sample confirms the photothermal stability of the system, suggesting no re-shaping of the AuNRs.[41–43]

The effect of the synthesised AuNRs on the viability of two cell lines, a human cervical cancer cell line (HeLa) and human fibroblasts (Fig. 3) was then studied. These cell lines were incubated for 24 h with several concentrations of both systems (modified and unmodified AuNRs). Two behaviours were observed. On the one hand, AuNR-PEG-r_8-k(cF) displayed no toxicity in HeLa cells at any of the concentrations tested (Fig. 3A), but negligible toxicity was detected in fibroblasts. On the other hand, naked AuNRs caused high toxicity in a dose-dependent manner (Fig. 3B) in both cell lines. For this reason, the complete removal of CTAB is mandatory. The lack of toxicity of modified AuNRs supports the notion that the modification of the AuNR surface is essential for complete CTAB elimination.

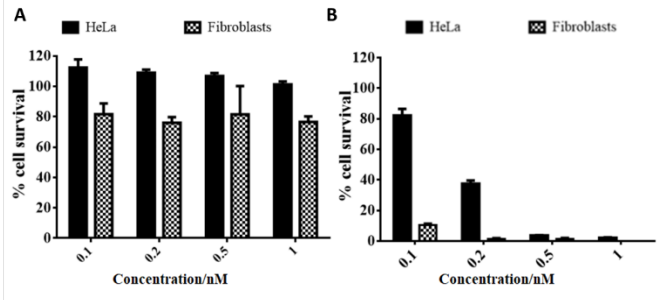

Fig. 3. Cell viability after 24 h incubation with different concentration of AuNRs: A) AuNR-PEG-r_8-k(cF) and B) unmodified AuNRs in HeLa and 3T3 fibroblasts cells.

Motivated by these results, the uptake properties of the system were explored by transmission electron microscopy (TEM) and by flow cytometry (Fig. 4, S6). For TEM experiments, HeLa cells were incubated with AuNR-PEG-r_8-k(cF) at 0.2 nM for 24 h.

Analysis of TEM images revealed that AuNRs were located in intracellular compartments, mainly vesicles (Fig. 4A, S6), which are in the range of 200-300 nm. Therefore, we hypothesise that, after 24 h incubation, rods were entrapped into late endosomes.[44] To quantify this translocation, we used flow cytometry, taking advantage of the cF present at the r_8 sequence. HeLa cells were incubated with various concentrations of AuNRs for 2 or 24 h. As shown in Fig. 4B, at the higher concentration assayed (1 nM), the amount of internalised AuNR-PEG-r_8-k(cF) increased 5-fold after 24h. When lower concentrations (0.2 nM) or time (2 h) were tested, the fluorescence of AuNR-PEG-r_8-k(cF) that was taken up could not be detected by flow cytometry.

We hypothesise that the acidic pH of the vesicle environment and the presence of intracellular membranes,[45,46] quench the fluorescence of the cF, making its detection more difficult. In fact, TEM analysis of cells incubated with 0.2 nM AuNR-PEG-r_8-k(cF) revealed internalization of the particles (Fig. 4A, S6).

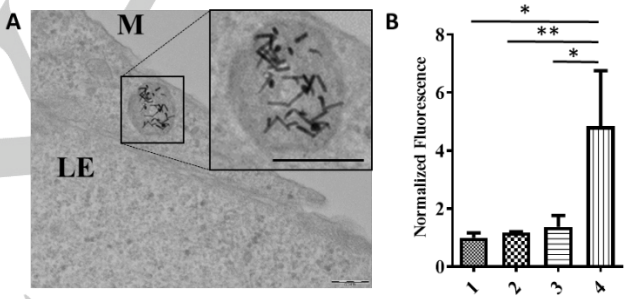

Fig. 4. A) Transmission electron micrograph of HeLa cells after a 24-h incubation with 0.2 nM AuNRs. M: cell membrane; LE: Late endosome; N: nucleus. Scale bar: 200 nm; B) Normalised fluorescence obtained by FACS when HeLa cells were incubated with different AuNR-PEG-r8-k(cF) concentrations during different times: 1) Control cells 2) 1 nM for 2 h; 3) 0.2 nM for 24 h and 4) 1 nM for 24 h. Values are reported as mean ± SEM (*P<0.05; **P<0.005; One-way ANOVA test).

After confirming the ability of our system to enter the cell, we tested its capacity to induce endosomal release. To this end, HeLa cells were incubated with a mixture of r_8-k(cF) peptide and the modified AuNR-PEG-r_8 system. We then irradiated them with CW laser, comparing various laser intensities and irradiation times. Cells were irradiated without media, which was added immediately after irradiation. The high thermal conductivity of water counterbalances the temperature increase caused by the irradiation. Solid supports with lower thermal conductivity lead to superior heating.[47] The concentration of the model peptide was 5000 times higher than that of the AuNR system. To quantify the effect of the irradiation, and given that r_8 has nuclear preference, the intensity of the fluorescence in the nucleus was studied. The selected laser intensities were 1.0, 4.5, 8.5 W/cm^2 for 2 min, and 4.5 W/cm^2 was evaluated at 2 and 4 min. As a control, cells with the peptide solution but not the AuNRs were irradiated at maximum time and power. We also analysed non-irradiated cells incubated with the peptide and the modified AuNR.

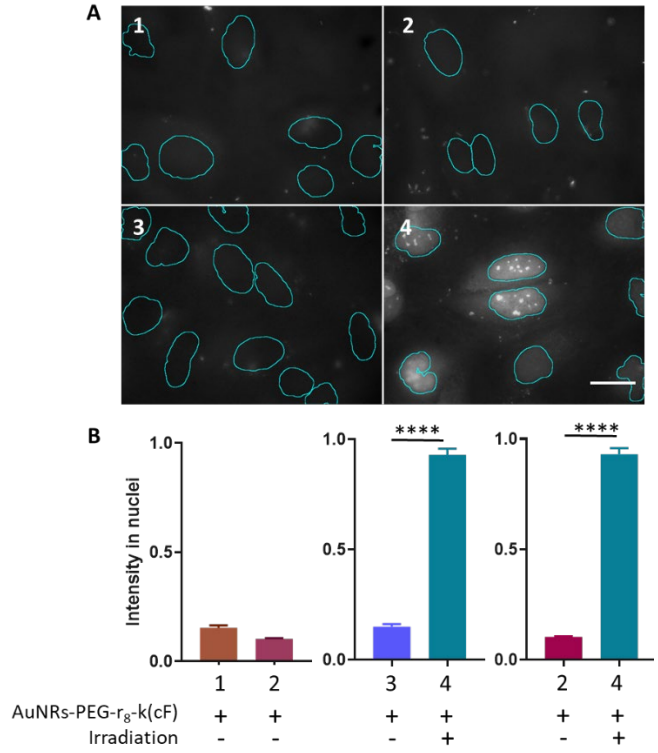

Fig. 5. A) Wide field images of HeLa cells incubated with 1) AuNRs-PEG-r_8-k(cF) before irradiation; 2) non irradiated AuNR-PEG-r_8-k(cF) after irradiation; 3) AuNR-PEG-r_8-k(cF) before irradiation; 4) irradiated AuNR-PEG-r_8-k(cF) after irradiation. Images display the green channel showing nuclei contour obtained from Hoechst labelling. B) Quantification of nuclei intensity of 1 vs 2, 3 vs 4 and 2 vs 4. Scale bar 25 µm.

Interestingly, fluorescence was detected in the nuclei in all the irradiated conditions, reaching a maximum at 2 min with 4.5 W/cm^2. Under irradiation for different periods, similar intensities were observed at each time point. With this data in hand, 2 min at 4.5 W/cm^2 was selected for further experiments. Of note, irradiation without the AuNR did not affect the peptide fate, which was detected only in the cytoplasmic region as a punctuated pattern (Fig. S7). We then compared the effect of irradiation on cells incubated with only AuNR-PEG-r_8-k(cF) (Fig. 5 and S8, S9) since AuNRs with nuclear targeting have been proposed as molecular probes for imaging since they can be detected by single-cell micro-Raman spectroscopy.[48] The fluorescence intensity of nuclei was measured before and after exposure to 2 min of laser irradiation at 4.5 W/cm^2. Again, non-irradiated cells were used as negative control. In this case, we detected the fluorescence of the cF of the peptide attached to the AuNR (Fig. 5A), which, after irradiation, mainly localised in the nucleus, as expected. As mentioned before, cF fluorescence is quenched at acidic pH, as in endocytic vesicles. Release of a cF labelled construct from the endosome to the cytosol and later re-localization to a given organelle can lead to saturation of the fluorescence signal (Fig. S8). To avoid this, and to allow quantification after irradiation, the imaging settings are adjusted taking as a reference the brighter images. Therefore, the fluorescence signal before irradiation is very subtle (Fig. 5, S9). Noteworthy, 24h after irradiation cells displayed normal morphology (Fig. S10).

To validate the potential of our strategy to deliver proteins through endosomes, BSA was selected as model protein due to its availability, medium size (66 KDa) and ease of functionalization. Additionally, BSA is not able to enter the cell itself, as is the case of most therapeutic proteins.

Initially, the model protein was modified in two steps. First, the solvent-exposed lysine residues were modified with GMBS (*N*-Succinimidyl 4-maleimidobutyrate) to introduce reactive maleimide groups, and then the D-Cys modified r_8 (cr_8) was added (Scheme S2A, Fig. S3). Amino acid analysis confirmed the conjugation of an average of 3.4 peptides/protein. To follow and quantify protein internalization, the dye Atto565, activated as *N*-hydroxysuccinimyl ester, was used to fluorescently label the protein.

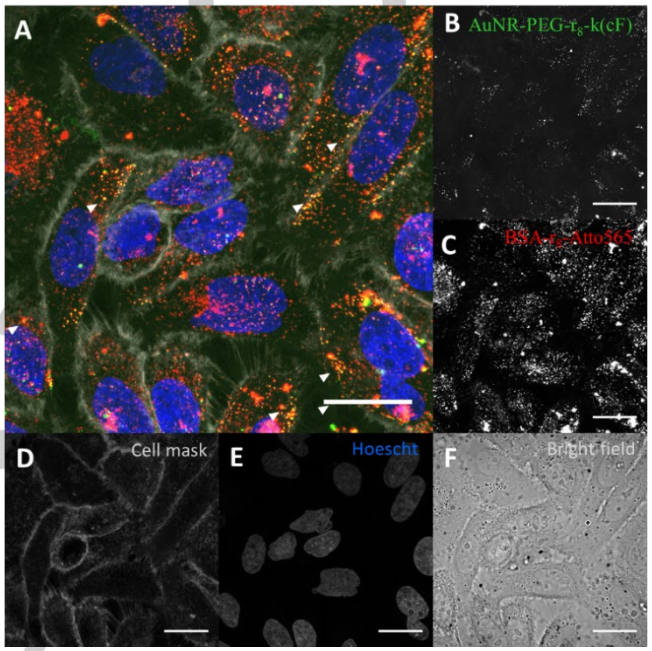

Fig. 6. z-stack projection of HeLa cells incubated with 1 nM of AuNR-PEG-r_8-k(cF) and 5µM BSA-$(r_8)_n$-Atto565 A) composite: in blue, Hoechst nuclei staining; in green: 1 nM of AuNR-PEG-r_8-k(cF); in red: 5µM BSA-r_8-Atto565; in grey: cell mask. B) Green channel, 1 nM of AuNR-PEG-r_8-k(cF). C) Red channel, 5µM BSA-$(r_8)_n$-Atto565. D) Cell mask; E) Hoechst nuclei staining; F) Bright Field. Scale bar 25 µm. µ-Slide 8 Well (ibidi, cat. number 80826) were used in all irradiation experiments.

To test whether BSA-$(r_8)_n$-Atto565 protein and AuNR-PEG-r_8-k(cF) internalise by the same mechanism, we incubated both with HeLa cells at a concentration of 5 µM and 1 nM respectively. Nuclear and cellular membrane counterstaining were used to locate them inside the cell and to probe its cytoplasmic localization by confocal microscopy, (Fig. 6A). Both the BSA-$(r_8)_n$-Atto565 protein and AuNR-PEG-r_8-k(cF) showed a punctuated pattern within the cell cytoplasm, suggesting that they entered the cells via endocytosis. Finally, when the images are merged (Fig. 6A), co-localization can be observed between protein and AuNR-PEG-r_8-k(cF) channels (overlap coefficient: r=0.823), thereby confirming that not only were the two entities able to enter by the same routes but some of them entered the same vesicles.

At this point, we queried whether laser irradiation would lead to the cytoplasmic release of the model protein. For this purpose, cells incubated with 5 µM BSA-$(r_8)_n$-Atto565 and 0.5 nM AuNR-PEG-r_8-k(cF) were irradiated with a CW NIR laser emitting at 1064 nm. Laser intensity and time were adjusted to 4.5 W/cm^2 and 2 min, respectively. Analysis by confocal microscopy revealed two well-differentiated areas (Fig. S11).

Cells from the non-irradiated area showed the same punctuated profile as those obtained before irradiation (Fig. 6) which suggests that both AuNR-PEG-r_8-k(cF) and BSA-$(r_8)_n$-Atto565 are able to enter the cells, where they remain trapped in the endosomes.

However, after NIR irradiation, the photothermal effect of the AuNR-PEG-r_8-k(cF) led to endosome disruption, causing the release of BSA-$(r_8)_n$-Atto565 (Fig. S11, S12 and S13). As expected, most of the two units (AuNRs and BSA) were found in the nucleus. Although the nuclear pore limits the entry of macromolecules, CPPs like cyclic-R_{10} or r_8 are able to use nuclear import mechanism to transport big proteins or other cargoes.[12,49] In addition, it has been reported that the nuclear pore protein complex can enlarge its diameter to 10-25 nm which is below the width of the AuNRs described in this work (9.0 ± 0.7 nm).[50,51] Therefore, modified BSA and AuNRs, when released, were translocated to the nucleus by the CPP. This experiment was performed in HeLa (Fig. S12) and fibroblast cells (Fig. S13), obtaining similar results.

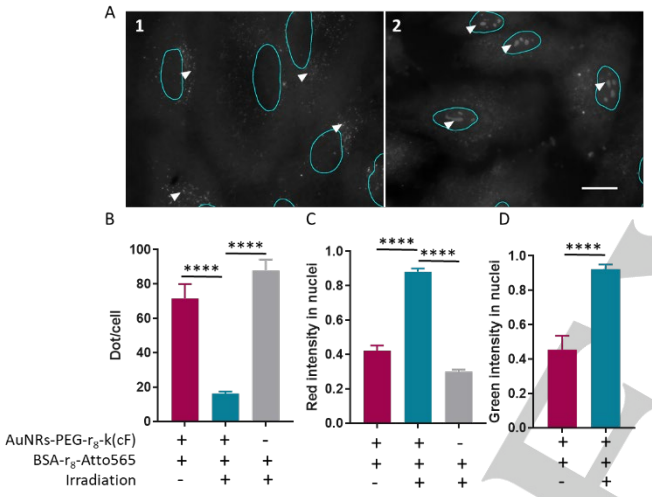

Fig. 7. A) Wide field images of HeLa cells incubated with BSA-r_8-Atto565 and AuNR-PEG-r_8-k(cF) (2h) 1) non-irradiated; 2) after irradiation. Images display the red channel showing nuclei contour obtained from Hoechst labelling. Quantification of B) number of dots/cell; C) red intensity in nuclei; D) green intensity in nuclei. White arrows mark endosomes in 1 and nucleoli in 2. Scale bar 20 µm

Having proved the potential of our strategy to deliver proteins to the intracellular environment, a more selective strategy was used to modify BSA in order to minimise possible side effects that could arise due to a non-selective strategy of functionalization. To this end, we took advantage of the free cysteine present in its sequence. One copy of r_8 was introduced as thioether by addition of the bromoacetyl *N*-terminal-modified peptide (Scheme S2B). MS analysis confirmed the introduction of only one copy of the peptide (Fig. S14). Fluorescent labelling with Atto565 allowed for the detection and quantification of the protein.

The introduction of only one r_8 copy has been described as sufficient to induce the cellular uptake of proteins.[52] The well-defined BSA-r_8 conjugate was then co-incubated with 0.01% of AuNR-PEG-r_8-k(cF) in Hela cells. After a 2-h incubation, cells were irradiated for 2 min at 4.5 W/cm^2. As previously seen with the release of r_8-k(cF) peptide, the number of cytoplasmic vesicles was reduced after irradiation, accompanied by an increase in the fluorescence intensity in the nuclei (Fig. 7, S15). Of note, 78-88% of cells displayed labelled nucleoli.

Conclusion

Here we describe the cytosolic delivery of a model protein with spatio-temporal control using a strategy that combines three elements: a CPP-modified protein, CPP-modified AuNRs and NIR irradiation. First, the CPP drives the internalization of the protein and the NP via endocytosis. Endosomal release of the CPP-modified systems is then achieved by NIR irradiation in the second biological window, which is preferred for biological applications. The superior photothermal properties of AuNRs allow for the use of a catalytic amount of NPs. Specifically, the protein:AuNR concentration ratio used in this work ranged from 5000:1 to 10000:1.

The modified AuNRs maintained their physical properties and were not cytotoxic before or after NIR laser irradiation. Under the optimised conditions, AuNR-PEG-r_8-k(cF) disrupted the endosomes/lysosomes and released the model protein into the cytoplasm, where it accumulated in the nucleus by the effect of the attached CPP. This strategy could be easily adapted to any protein. Importantly, site-specific modification of the protein is not required, although it can be applied, as demonstrated by the delivery of both BSA-$(r_8)_n$ and BSA-r_8. The described approach holds enormous potential for the intracellular delivery of proteins to a specific organelle, as demonstrated for the nucleus, and could be used to study or manipulate cell function.

Acknowledgements

This work was funded by MINECO-FEDER (BIO2016-75327-R), the Generalitat de Catalunya (XRB, 2017SGR0998 and CERCA Programme), by Fondap 15130011, by IN^{2}UB (ART2019-25173) and with the support of LCF/PR/GN14/10270002 - "la Caixa" Foundation. IRB Barcelona is the recipient of a Severo Ochoa Award of Excellence from MINECO (Government of Spain).

Keywords: Gold nanorod • Near-infrared irradiation • cytosolic delivery • cell-penetrating peptide

[1] J. A. Doudna, E. Charpentier, *Science (80-.).* **2014**, *346*, 1258096.
[2] M. Swierczewska, K. C. Lee, S. Lee, *Expert Opin. Emerg. Drugs* **2015**, *20*, 531–536.
[3] M. P. Stewart, A. Sharei, X. Ding, G. Sahay, R. Langer, K. F. Jensen, *Nature* **2016**, *538*, 183–192.
[4] S.-O. Choi, Y.-C. Kim, J. W. Lee, J.-H. Park, M. R. Prausnitz, M. G. Allen, *Small* **2012**, *8*, 1081–1091.
[5] B. R. McNaughton, J. J. Cronican, D. B. Thompson, D. R. Liu, *Proc. Natl. Acad. Sci.* **2009**, *106*, 6111 LP – 6116.
[6] F. Scaletti, J. Hardie, Y.-W. Lee, D. C. Luther, M. Ray, V. M. Rotello, *Chem. Soc. Rev.* **2018**, *47*, 3421–3432.
[7] H. Räägel, P. Säälik, M. Pooga, *Biochim. Biophys. Acta* **2010**, *1798*, 2240—2248.
[8] M. Lundberg, M. Johansson, *Biochem. Biophys. Res. Commun.* **2002**, *291*, 367–371.
[9] I. Nakase, M. Niwa, T. Takeuchi, K. Sonomura, N. Kawabata, Y. Koike, M. Takehashi, S. Tanaka, K. Ueda, J. C. Simpson, A. T. Jones, Y. Sugiura, S. Futaki, *Mol. Ther.* **2004**, *10*, 1011–1022.
[10] R. Fischer, M. Fotin-Mleczek, H. Hufnagel, R. Brock, *ChemBioChem* **2005**, *6*, 2126–2142.

[11] A. El-Sayed, S. Futaki, H. Harashima, *AAPS J.* **2009**, *11*, 13–22.
[12] H. D. Herce, D. Schumacher, A. F. L. Schneider, A. K. Ludwig, F. A. Mann, M. Fillies, M.-A. Kasper, S. Reinke, E. Krause, H. Leonhardt, M. C. Cardoso, C. P. R. Hackenberger, *Nat. Chem.* **2017**, *9*, 762–771.
[13] J. S. Wadia, R. V Stan, S. F. Dowdy, *Nat. Med.* **2004**, *10*, 310–315.
[14] M. Akishiba, T. Takeuchi, Y. Kawaguchi, K. Sakamoto, H.-H. Yu, I. Nakase, T. Takatani-Nakase, F. Madani, A. Gräslund, S. Futaki, *Nat. Chem.* **2017**, *9*, 751–761.
[15] M. Sánchez-Navarro, M. Teixidó, E. Giralt, *Nat. Chem.* **2017**, *9*, DOI 10.1038/nchem.2837.
[16] M. Matsushita, H. Noguchi, Y.-F. Lu, K. Tomizawa, H. Michiue, S.-T. Li, K. Hirose, S. Bonner-Weir, H. Matsui, *FEBS Lett.* **2004**, *572*, 221–226.
[17] W. Jerjes, T. A. Theodossiou, H. Hirschberg, A. Høgset, A. Weyergang, P. K. Selbo, Z. Hamdoon, C. Hopper, K. Berg, *J. Clin. Med.* **2020**, *9*, 528.
[18] M. M. Lino, L. Ferreira, *Drug Discov. Today* **2018**, *23*, 1062–1070.
[19] M. Kim, J.-H. Lee, J.-M. Nam, *Adv. Sci. (Weinheim, Baden-Wurttemberg, Ger.* **2019**, *6*, 1900471.
[20] E. C. Dreaden, A. M. Alkilany, X. Huang, C. J. Murphy, M. A. El-Sayed, *Chem. Soc. Rev.* **2012**, *41*, 2740–2779.
[21] X. Huang, P. K. Jain, I. H. El-Sayed, M. A. El-Sayed, *Lasers Med. Sci.* **2007**, *23*, 217.
[22] E. Hemmer, A. Benayas, F. Légaré, F. Vetrone, *Nanoscale Horizons* **2016**, *1*, 168–184.
[23] H. Chen, L. Shao, Q. Li, J. Wang, *Chem. Soc. Rev.* **2013**, *42*, 2679–2724.
[24] J. Shen, H.-C. Kim, C. Mu, E. Gentile, J. Mai, J. Wolfram, L. Ji, M. Ferrari, Z. Mao, H. Shen, *Adv. Healthc. Mater.* **2014**, *3*, 1629–1637.
[25] B.-K. Wang, X.-F. Yu, J.-H. Wang, Z.-B. Li, P.-H. Li, H. Wang, L. Song, P. K. Chu, C. Li, *Biomaterials* **2016**, *78*, 27–39.
[26] M. M. Lino, S. Simões, S. Pinho, L. Ferreira, *Nanoscale* **2017**, *9*, 18668–18680.
[27] S. Futaki, T. Suzuki, W. Ohashi, T. Yagami, S. Tanaka, K. Ueda, Y. Sugiura, *J. Biol. Chem.* **2001**, *276*, 5836–5840.
[28] R. M. Martin, G. Ter-Avetisyan, H. D. Herce, A. K. Ludwig, G. Lättig-Tünnemann, M. C. Cardoso, *Nucleus* **2015**, *6*, 314–325.
[29] L. Vigderman, E. R. Zubarev, *Chem. Mater.* **2013**, *25*, 1450–1457.
[30] B. Nikoobakht, M. A. El-Sayed, *Chem. Mater.* **2003**, *15*, 1957–1962.
[31] A. M. Alkilany, P. K. Nagaria, C. R. Hexel, T. J. Shaw, C. J. Murphy, M. D. Wyatt, *Small* **2009**, *5*, 701–708.
[32] C. Kinnear, H. Dietsch, M. J. D. Clift, C. Endes, B. Rothen-Rutishauser, A. Petri-Fink, *Angew. Chemie Int. Ed.* **2013**, *52*, 1934–1938.
[33] M. M. Fretz, N. A. Penning, S. Al-Taei, S. Futaki, T. Takeuchi, I. Nakase, G. Storm, A. T. Jones, *Biochem. J.* **2007**, *403*, 335–342.
[34] J. B. Rothbard, S. Garlington, Q. Lin, T. Kirschberg, E. Kreider, P. L. McGrane, P. A. Wender, P. A. Khavari, *Nat. Med.* **2000**, *6*, 1253–1257.
[35] Z. Niu, E. Samaridou, E. Jaumain, J. Coëne, G. Ullio, N. Shrestha, J. Garcia, M. Durán-Lobato, S. Tovar, M. J. Santander-Ortega, M. V. Lozano, M. M. Arroyo-Jimenez, R. Ramos-Membrive, I. Peñuelas, A. Mabondzo, V. Préat, M. Teixidó, E. Giralt, M. J. Alonso, *J. Control. Release* **2018**, *276*, 125–139.
[36] Y. Kawaguchi, T. Takeuchi, K. Kuwata, J. Chiba, Y. Hatanaka, I. Nakase, S. Futaki, *Bioconjug. Chem.* **2016**, *27*, 1119–1130.
[37] L. Tong, J.-X. Cheng, *Nanomedicine* **2009**, *4*, 265–276.
[38] A. L. Riveros, C. Eggeling, S. Riquelme, C. Adura, C. López-Iglesias, F. Guzmán, E. Araya, M. Almada, J. Juárez, M. A. Valdez, I. A. Fuentevilla, O. López, M. J. Kogan, *Int. J. Nanomedicine* **2020**, *15*, 1837–1851.
[39] F. Morales-Zavala, H. Arriagada, N. Hassan, C. Velasco, A. Riveros, A. R. Álvarez, A. N. Minniti, X. Rojas-Silva, L. L. Muñoz, R. Vasquez, K. Rodriguez, M. Sanchez-Navarro, E. Giralt, E. Araya, R. Aldunate, M. J. Kogan, *Nanomedicine Nanotechnology, Biol. Med.* **2017**, *13*, DOI 10.1016/j.nano.2017.06.013.
[40] C. Velasco-Aguirre, F. Morales-Zavala, E. Salas-Huenuleo, E. Gallardo-Toledo, O. Andonie, L. Muñoz, X. Rojas, G. Acosta, M. Sánchez-Navarro, E. Giralt, E. Araya, F. Albericio, M. J. Kogan, *Nanomedicine* **2017**, *12*, DOI 10.2217/nnm-2017-0181.
[41] A. B. Taylor, A. M. Siddiquee, J. W. M. Chon, *ACS Nano* **2014**, *8*, 12071–12079.
[42] D. Harris-Birtill, M. Singh, Y. Zhou, A. Shah, P. Ruenraroengsak, M. E. Gallina, G. B. Hanna, A. E. G. Cass, A. E. Porter, J. Bamber, D. S. Elson, *PLoS One* **2017**, *12*, e0185990.
[43] W. J. Kennedy, S. Izor, B. D. Anderson, G. Frank, V. Varshney, G. J. Ehlert, *ACS Appl. Mater. Interfaces* **2018**, *10*, 43865–43873.
[44] I. G. Ganley, K. Carroll, L. Bittova, S. Pfeffer, *Mol. Biol. Cell* **2004**, *15*, 5420–5430.
[45] P. Ruzza, B. Biondi, A. Marchiani, N. Antolini, A. Calderan, *Pharmaceuticals* **2010**, *3*, 1045–1062.
[46] J.-M. Swiecicki, F. Thiebaut, M. Di Pisa, S. Gourdin -Bertin, J. Tailhades, C. Mansuy, F. Burlina, S. Chwetzoff, G. Trugnan, G. Chassaing, S. Lavielle, *Sci. Rep.* **2016**, *6*, 20237.
[47] C.-H. Chou, C.-D. Chen, C. R. C. Wang, *J. Phys. Chem. B* **2005**, *109*, 11135–11138.
[48] A. K. Oyelere, P. C. Chen, X. Huang, I. H. El-Sayed, M. A. El-Sayed, *Bioconjug. Chem.* **2007**, *18*, 1490–1497.
[49] H. D. Herce, A. E. Garcia, M. C. Cardoso, *J. Am. Chem. Soc.* **2014**, *136*, 17459–17467.
[50] T. D. Allen, J. M. Cronshaw, S. Bagley, E. Kiseleva, M. W. Goldberg, *J. Cell Sci.* **2000**, *113*, 1651 LP – 1659.
[51] A. Chugh, F. Eudes, Y.-S. Shim, *IUBMB Life* **2010**, *62*, 183–193.
[52] S. G. Patel, E. J. Sayers, L. He, R. Narayan, T. L. Williams, E. M. Mills, R. K. Allemann, L. Y. P. Luk, A. T. Jones, Y.-H. Tsai, *Sci. Rep.* **2019**, *9*, 6298.

Entry for the Table of Contents

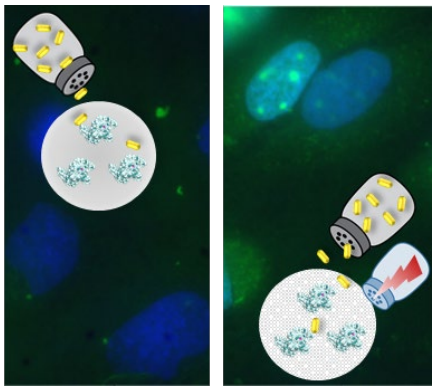

The inability of most proteins to transverse the cellular membrane hampers the development of protein therapeutics for intracellular targets. In this work, we describe the use of catalytic amounts of gold nanorods combined with near infrared laser irradiation as a strategy to trigger cytosolic delivery of proteins.